Coupled maps on fractal lattices

Mario G. Cosenza and Raymond Kapral
Chemical Physics Theory Group, Department of Chemistry, University of Toronto, Toronto, Canada M5S 1A1
(Received 18 February 1992)

A fractal array of coupled maps, where space is nonuniform, is considered as a dynamical system. The stability and bifurcations of spatially synchronized, periodic states on the Sierpinski gasket are studied. The matrix that expresses the coupling among neighboring elements exhibits a spectrum of eigenvalues with multifractal properties, and their global scaling behavior is characterized by the function $f(\alpha)$. The multifractal character of the eigenvalues affects the stability boundaries of the synchronized, periodic states in the parameter plane of the system. The boundary structure allows access to regions of stability and gives rise to bifurcations that are not present in regular lattices.

PACS number(s): 05.45.+b, 47.20.Ky, 82.20.Wt

I. INTRODUCTION

Coupled-map lattices are discrete space-time dynamical systems comprised of a coupled array of discrete-time maps. The study of these systems has proved interesting in a number of contexts. Viewed as general spatially distributed dynamical systems, it has been shown that they display much of the phenomenology observed in nature; for example, turbulence, intermittency, and syncrhonization [1]. Properly constructed, they also provide faithful models of specific physical phenomena or partial differential equations that can be simulated very efficiently [2].

In these investigations of coupled-map lattices (CML's), the underlying lattice on which the dynamics is defined has invariably been a regular lattice. It is now well established that a variety of interesting physical processes take place on objects with a fractal structure [3]. Examples of such processes include phase transitions [4], random walks [5], and reaction diffusion dynamics [6]. In view of the physical relevance and ubiquity of such processes, it is useful to study coupled-map systems defined on fractal lattices both as abstract dynamical systems and models for some of the above-mentioned physical phenomena. The discrete diffusion coupling on fractal lattices is a natural form for the coupling in these spatially inhomogeneous structures. This gives added relevance to the investigation of these dynamical systems.

This paper presents a study of coupled-map fractal lattices (CMFL's). The full range of phenomena exhibited by these dynamical systems is not explored, rather the focus is on a specific fractal lattice, the Sierpinski gasket, and one class of dynamical states, the spatially synchronized period-doubled orbits. In particular, we study the stability domains of these states and their scaling properties as well as the inhomogeneous states to which they bifurcate. New features arise as a consequence of the fractal character of space.

A general basis and notation for the treatment of deterministic fractal structures as CML models are introduced in Sec. II. The coupling among the neighboring sites of the lattice is described by a matrix, which exhibits a self-similar structure. In Sec. III, the spectrum of eigenvalues and eigenvectors is analyzed. The eigenvalues can be found from a map that relates any two consecutive levels of construction of the lattice [7]. A subset of eigenvalues of the coupling matrix possesses multifractal properties, and its spectrum of singularities is calculated in Sec. IV. In Sec. V we derive the corresponding maps for the eigenvalues of the matrix expressing diffusion coupling in one- and two-dimensional regular arrays, and compare their scaling properties with those of the map for the fractal lattice. The bifurcation structure of synchronized states is analyzed in Sec. VI for a local dynamics given by the logistic map. The multifractal character of the eigenvalues of the coupling matrix affects the boundaries of the stability regions in the parameter plane of the synchronized, periodic states. The spatial patterns that form as a result of bifurcations from the synchronized states are studied. The conclusions of the paper are presented in Sec. VII.

II. COUPLED MAPS ON THE SIERPINSKI GASKET

The triangular Sierpinski gasket is a deterministic fractal. At the nth level of construction, each of the 3^n elements or cells of the gasket can be specified by a sequence of symbols $\boldsymbol{\alpha}_n = (\alpha_1 \alpha_2 \ldots \alpha_n)$, where $\alpha_i \in \{1,2,3\}$. At level $n+1$, each triangular cell $(\alpha_1 \ldots \alpha_n)$ is subdivided into three smaller triangles, which are now labeled $\boldsymbol{\alpha}_{n+1} = (\alpha_1 \ldots \alpha_n \alpha_{n+1})$, where the first n elements of the sequence, $\alpha_1 \ldots \alpha_n$, are the same as the mother cell (Fig. 1).

A sequence $\boldsymbol{\alpha}_n = (\alpha_1 \ldots \alpha_n)$ can be written as $(\alpha_1 \ldots \alpha_{n-s} \alpha_{n-s+1}^s)$, for some $s \in \{1,2,\ldots,n\}$, where α_i^s stands for the product of s factors α_i. The neighbors of the cell with this sequence are labeled $\boldsymbol{\alpha}_n' = (\alpha_1 \ldots \alpha_{n-1} \alpha_n + 1)$, $\boldsymbol{\alpha}_n'' = (\alpha_1 \ldots \alpha_{n-1} \alpha_n + 2)$, and $\overline{\boldsymbol{\alpha}} = (\alpha_1 \ldots \alpha_{n-s+1} \alpha_{n-s}^s)$, where the addition $\alpha_i + j$ is to be carried out modulo 3 here and in the sequel. The first two labels specify the two neighbors of $(\alpha_1 \ldots \alpha_n)$

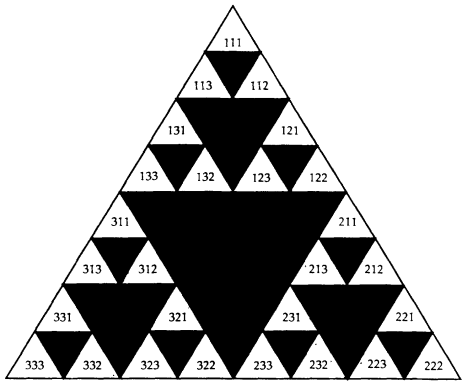

FIG. 1. Sierpinski gasket at level $n = 3$, showing labels on the cells.

which lie in the same mother cell (the first $n-1$ indices are $\alpha_1 \ldots \alpha_{n-1}$) while the third label specifies a neighbor lying in a different mother cell. If $s = n$, then the cell is a vertex, labeled by (α_1^n), and it has only two neighbors belonging to the same mother cell.

The dynamical system considered in this paper is constructed by associating a nonlinear function with each cell of the Sierpinski gasket and coupling these functions through nearest-neighbor diffusion interactions [8]. At a level of generation specified by the parameter n, the space-time evolution of the system is described by the 3^n equations in backward or forward difference forms, respectively, as

$$\begin{aligned} x(\boldsymbol{\alpha}_n, t+1) &= f(x(\boldsymbol{\alpha}_n, t); \lambda) \\ &\quad + \gamma[x(\boldsymbol{\alpha}_n', t) + x(\boldsymbol{\alpha}_n'', t) + x(\overline{\boldsymbol{\alpha}}_n, t) \\ &\quad - 3x(\boldsymbol{\alpha}_n, t)], \end{aligned} \tag{1a}$$

$$\begin{aligned} x(\boldsymbol{\alpha}_n, t+1) &= (1-3\gamma) f(x(\boldsymbol{\alpha}_n, t); \lambda) \\ &\quad + \gamma[f(x(\boldsymbol{\alpha}_n', t); \lambda) + f(x(\boldsymbol{\alpha}_n'', t); \lambda) \\ &\quad + f(x(\overline{\boldsymbol{\alpha}}_n, t); \lambda)], \end{aligned} \tag{1b}$$

where $x(\boldsymbol{\alpha}_n, t)$ gives the state of the cell labeled $(\alpha_1 \ldots \alpha_n)$ on a lattice containing 3^n elements at discrete time t; $f(x; \lambda)$ is a (nonlinear) function that specifies the local dynamics and depends on some parameter λ; γ is a parameter that determines the strength of the coupling among nearest neighbors. Equations (1a) and (1b) may be written in matrix form, respectively, as

$$\mathbf{x}_n(t+1) = \mathbf{f}(\mathbf{x}_n(t); \lambda) + \gamma \mathbf{M}_n \mathbf{x}_n(t), \tag{2a}$$

$$\mathbf{x}_n(t+1) = \mathbf{f}(\mathbf{x}_n(t); \lambda) + \gamma \mathbf{M}_n \mathbf{f}(\mathbf{x}_n(t); \lambda). \tag{2b}$$

The 3^n components of $\mathbf{x}_n$ may be ordered as follows. Let $i = 1, \ldots, 3^n$ be an integer index associated with a cell on the fractal so that each cell sequence $(\alpha_1 \ldots \alpha_n)$ corresponds to a value of i. If at a level n the ith component of $\mathbf{x}_n$ is $x_n(i) = x(\alpha_1 \ldots \alpha_n)$, then at level $n+1$ we choose

$$\begin{aligned} x_{n+1}(3i-2) &= x(\alpha_1 \ldots \alpha_n, 1), \\ x_{n+1}(3i-1) &= x(\alpha_1 \ldots \alpha_n, 2), \\ x_{n+1}(3i) &= x(\alpha_1 \ldots \alpha_n, 3). \end{aligned} \tag{3}$$

Using this scheme and starting with $x_1(1) = x(1), x_1(2) = x(2), x_1(3) = x(3)$, the association of i with a sequence $(\alpha_1 \ldots \alpha_n)$ is uniquely determined. Given this notation, the ith component of the vector-valued function $\mathbf{f}$ is $f(x_n(i))$. The matrix $\mathbf{M}_n$ is a $3^n \times 3^n$ real, symmetric matrix which expresses the coupling among the components $\{x_n(i)\}$. With this ordering, the self-similar structure of the coupling matrix is manifest: for $r = 1, \ldots, n-1$, $\mathbf{M}_n$ consists of 3^{n-r} diagonal blocks of size $3^r \times 3^r$ corresponding to elements $M_n(i,j) = M(\alpha_1 \ldots \alpha_{n-r} \ldots \alpha_n, \beta_1 \ldots \beta_{n-r} \ldots \beta_n)$ such that $\alpha_k = \beta_k$ $(k = 1, \ldots, n-r)$, with coupling among these blocks,

$$M(\alpha_1 \ldots \alpha_{n-r} \ldots \alpha_{n-r+1}^r, \alpha_1 \ldots \alpha_{n-r+1}\, \alpha_{n-r}^r) = 1, \tag{4}$$

and the elements of the smallest blocks $(r = 1)$ being

$$M(\boldsymbol{\alpha}_n, \boldsymbol{\alpha}_n') = M(\boldsymbol{\alpha}_n, \boldsymbol{\alpha}_n'') = M(\boldsymbol{\alpha}_n', \boldsymbol{\alpha}_n'') = 1, \tag{5}$$

$$M(\boldsymbol{\alpha}_n, \boldsymbol{\alpha}_n) = \begin{cases} -2 \text{ if } \boldsymbol{\alpha}_n = (\alpha_1^n) \\ -3 \text{ if } \boldsymbol{\alpha}_n \neq (\alpha_1^n). \end{cases} \tag{6}$$

III. SPECTRUM OF $\mathbf{M}_n$

As a preliminary to considering the bifurcation structure of Eqs. (2a) and (2b), it is useful to study the eigenvalue problem for the matrix $\mathbf{M}_n$. The analysis is equivalent to the study of normal modes on a fractal lattice, which figures prominently in calculations of the spectral dimension [9]. The calculation presented below bears a relation to the earlier investigation of Rammal [7] for nearest-neighbor coupling of the vertices joining the cells of a Sierpinski gasket. In our CMFL model the nodes are the cells of the lattice and each map is coupled to three neighbors. Hence, the derivation and focus are rather different and the presentation is given in some detail. In addition, we shall concentrate on the dynamical system and multifractal aspects of the analysis.

Assume that at a given level n there are ν_n different eigenvalues of $\mathbf{M}_n$, denoted by $\mu_n(j)$, $j = 1, 2, \ldots, \nu_n$. The degree of degeneracy of the eigenvalue $\mu_n(j)$ will be denoted by $g_n(\mu(j)) \equiv g_n(j)$, so that $\sum_j g_n(j) = 3^n$. Let $\{\mathbf{u}_n(i) : i = 1, 2, \ldots, 3^n\}$ be the complete set of orthonormal eigenvectors of $\mathbf{M}_n$. We shall denote by $\{\mathbf{u}_n^{(k)}(j) : k = 1, 2, \ldots, g_n(j)\}$ the set of eigenvectors associated with $\mu_n(j)$:

$$\mathbf{M}_n \mathbf{u}_n^{(k)}(j) = \mu_n(j) \mathbf{u}_n^{(k)}(j). \tag{7}$$

For a given vector $\mathbf{u}_n^{(k)}(j)$, Eq.(7) consists of 3^n equations of the form

$$\begin{aligned} (\mu+2)u(\boldsymbol{\alpha}) &= u(\boldsymbol{\alpha}') + u(\boldsymbol{\alpha}') && \text{if } \boldsymbol{\alpha} = (\alpha_1^n), \\ (\mu+3)u(\boldsymbol{\alpha}) &= u(\boldsymbol{\alpha}') + u(\boldsymbol{\alpha}'') + u(\overline{\boldsymbol{\alpha}}) && \text{if } \boldsymbol{\alpha} \neq (\alpha_1^n). \end{aligned} \tag{8}$$

We drop the subscript n when it is not explicitly used.

The *spatially homogeneous* mode has eigenvalue $\mu = 0$, and $u(\alpha_1 \ldots \alpha_n) = 3^{-n/2}, \forall \alpha_1, \ldots, \alpha_n$. Since the eigen-

vectors are mutually orthogonal, all other modes must satisfy $\sum_{\alpha_1,\ldots,\alpha_n} u(\alpha_1 \ldots \alpha_n) = 0$.

In addition to the homogeneous mode, we can show that for $n > 1$, two basic modes are always present. These two modes will determine the structure of the spectrum of $\mathbf{M}_n$ as the superposition of two distinct parts, each associated with one of the basic modes.

Symmetric modes have $\mu = -3$, and

$$u(\boldsymbol{\alpha}) + u(\boldsymbol{\alpha}') + u(\boldsymbol{\alpha}'') = 0, \quad u(\boldsymbol{\alpha}) = u(\overline{\boldsymbol{\alpha}}). \tag{9}$$

Let $g_n(-3)$ be the degree of degeneracy of these modes at level n, i.e., the minimum number of variables needed to specify a vector obeying conditions (9) for given n. Level $n+1$ consists of three gaskets corresponding to a level of construction n, coupled through three pairs of cells, each of these pairs satisfying $u(\alpha_1\alpha_2^n) = u(\alpha_2\alpha_1^n)$. Therefore, the degeneracy of these modes at level $n+1$ gives the number of variables needed to specify each of the three level-n gaskets, minus three variables determined by the coupling of these gaskets. Thus $g_{n+1}(-3) = 3g_n(-3) - 3$, and for any $n \geq 1$, one can derive

$$g_n(-3) = \frac{3^{n-1}+3}{2}. \tag{10}$$

Antisymmetric modes have $\mu = -5$, and

$$u(\boldsymbol{\alpha}) + u(\boldsymbol{\alpha}') + u(\boldsymbol{\alpha}'') = 0, \quad u(\boldsymbol{\alpha}) = -u(\overline{\boldsymbol{\alpha}}). \tag{11}$$

For these modes, $u(\alpha_1^n) = 0$. The level of construction $n+1$ consists of three level-n gaskets, coupled through three pairs of cells which no longer have vanishing values but satisfy $u(\alpha_1\alpha_2^n) = -u(\alpha_2\alpha_1^n)$. The vertices of each gasket have the property $u(\alpha_1^{n+1}) + u(\alpha_1(\alpha_1+1)^n) + u(\alpha_1(\alpha_1+2)^n) = 0$, where $(\alpha_1(\alpha_1+1)^n)$ and $(\alpha_1(\alpha_1+2)^n)$ are cells coupled to the other two gaskets. Therefore the three pairs of cells coupling the three level-n gaskets are determined by one variable. Thus $g_{n+1}(-5) = 3g_n(-5) + 1$, and for $n \geq 1$,

$$g_n(-5) = \frac{3^{n-1}-1}{2}. \tag{12}$$

Before carrying out a general analysis of the eigenvalue problem, it is instructive to examine the level $n = 2$. Equations (8) for $n = 2$ can be solved by introducing the quantities

$$\begin{aligned} c(1) &= u(11) + u(22) + u(33), \\ c(2) &= u(12) + u(23) + u(31), \\ c(3) &= u(13) + u(21) + u(32). \end{aligned} \tag{13}$$

In terms of these variables, Eqs. (8) for $n = 2$ can be reduced to

$$\begin{aligned} (\mu+2)c(1) &= c(2) + c(3), \\ (\mu+3)c(2) &= c(1) + 2c(3), \\ (\mu+3)c(3) &= c(1) + 2c(2), \end{aligned} \tag{14}$$

which have nontrivial solutions if $\mu(\mu+3)(\mu+5) = 0$. Furthermore,

$$u(\alpha_1\alpha_2) = \text{const} \iff \mu = 0, \quad \forall \alpha_1, \alpha_2$$

$$c(1) + c(2) + c(3) = 0,$$

$$\begin{aligned} c(2) = c(3) \neq 0,\ c(1) \neq 0 &\Leftrightarrow \mu = -3 \\ c(2) \neq c(3),\ c(1) = 0 &\Leftrightarrow \mu = -5. \end{aligned}$$

(15)

On the other hand, if all $c(\alpha_1) = 0$, the number of equations in (8) can be reduced to three:

$$\begin{aligned} (\mu+2)[u(22)+u(33)] &= [u(21)+u(31)] \\ &\quad +[u(23)+u(32)], \\ (\mu+2)[u(23)+u(32)] &= [u(21)+u(31)] \\ &\quad +[u(22)+u(33)], \\ (\mu+4)[u(21)+u(31)] &= [u(22)+u(33)]. \end{aligned} \tag{16}$$

The requirement of nontrivial solutions yields the condition

$$(\mu+3)(\mu^2+5\mu+3) = 0. \tag{17}$$

A condition identical to (17) is obtained if trivial solutions to Eq. (16) are admitted. Thus, the different eigenvalues and their degeneracies for $n = 2$ can be found by using the definitions (13). At level $n = 1$, the possible eigenvalues are $\mu_1 = 0, -3$. The eigenvalues corresponding to $n = 2$ contain those of $n = 1$, in addition to the ones given by the transformation $\mu_1 = \mu_2(\mu_2+5)$. The eigenvalues and eigenvectors given by Eqs. (16) and (17) may be expressed as

$$\left.\begin{matrix} c(\alpha_1) = 0 \\ \sum_{\alpha_2} u(\alpha_1\alpha_2) \neq 0 \end{matrix}\right\} \Leftrightarrow \mu \equiv \xi(\sigma_1) = \frac{-5 \pm \sqrt{25+4\xi_0}}{2}, \tag{18}$$

where $\xi_0 \equiv -3$ and σ_1 stands for a binary symbol; we choose $\sigma_1 = 0$ (or 1) if the $+$ (or $-$) sign is taken in expression (18).

The procedure for $n = 2$ suggests an iterative approach for obtaining eigenvalues and eigenvectors at successive levels of construction of the lattice. Consider Eqs. (8) at level $n+1$ and suppose that the eigenvalues at level n are known. The 3^{n+1} equations (8) for the components $u(\alpha_1 \ldots \alpha_{n+1})$ at a level $n+1$ can be reduced to 3^n equations for 3^n variables consisting of combinations of the $u(\alpha_1 \ldots \alpha_{n+1})$'s. The eigenvalues obtained from this reduced system of 3^n equations contain the eigenvalues corresponding to level n and new ones corresponding to level $n+1$, obtained by the relation

$$\mu_n = \mu_{n+1}(\mu_{n+1}+5). \tag{19}$$

The same relation applies for diffusion coupling of the vertices joining the cells of the Sierpinski gasket [7]. Here we present a scheme for generating all the eigenvalues, their degeneracies and corresponding eigenmodes at any level n. Let $m = 1, 2, \ldots, n-1$, and define for each m

$$c_n(\alpha_1 \dots \alpha_{n-m}) \equiv \sum_{i=0}^{2} c_n(1+i, \alpha_1 + i, \dots, \alpha_{n-m} + i),$$

$$\forall \alpha_1, \dots, \alpha_{n-m}, \quad (20)$$

with the convention $c_n(\alpha_1 \dots \alpha_n) = u(\alpha_1 \dots \alpha_n)$.

Equation (20) represents n sets of definitions, each set containing 3^{n-m} quantities. For a given m, Eqs. (8) can be combined to yield a reduced system of 3^{n-m} equations in terms of the set of 3^{n-m} quantities $c_n(\alpha_1 \dots \alpha_{n-m})$. The requirement of nontrivial solutions for these variables at each step m leads to two families of eigenvalues, $\mu_n(j) \in \{\xi(\sigma_1 \sigma_2 \dots)\}$ or $\mu_n(j) \in \{\eta(\sigma_1 \sigma_2 \dots)\}$, where $\sigma_i \in \{0, 1\}$, which can be found as follows.

Let $r = n - m$, and take m in decreasing order, i.e., $r = 1, \dots, n-1$. For $r = 0$, we consider the condition

$$\sum_{\alpha_1} c_n(\alpha_1) = 0,$$

$$\begin{aligned} c_n(1) \neq 0, &\Leftrightarrow \xi_0 = -3 \\ c_n(1) = 0, &\Leftrightarrow \eta_0 = -5\,. \end{aligned} \quad (21)$$

For $r = 1$ to $n-2$,

$$c_n(\alpha_1 \dots \alpha_r) = 0,$$

$$\begin{aligned} c_n(1 \dots \alpha_{r+1}) \neq 0 &\Leftrightarrow \xi(\sigma_1 \dots \sigma_r) \\ c_n(1 \dots \alpha_{r+1}) = 0 &\Leftrightarrow \eta(\sigma_1 \dots \sigma_r), \end{aligned} \quad (22)$$

and for $r = n-1$,

$$c_n(\alpha_1 \dots \alpha_{n-1}) = 0 \Leftrightarrow \xi(\sigma_1 \dots \sigma_{n-1}), \quad (23)$$

where both families $\{\xi_n(\sigma_1 \dots \sigma_r)\}$ or $\{\eta_n(\sigma_1 \dots \sigma_r)\}$ can be generated from the recursive relations

$$\eta(\sigma_1 \dots \sigma_{r+1}) = \frac{-5 \pm \sqrt{25 + 4\eta(\sigma_1 \dots \sigma_r)}}{2},$$

$$r = 0, \dots, n-2; \quad (24)$$

$$\xi(\sigma_1 \dots \sigma_{r+1}) = \frac{-5 \pm \sqrt{25 + 4\xi(\sigma_1 \dots \sigma_r)}}{2},$$

$$r = 0, \dots, n-1; \quad (25)$$

with $\sigma_i = 0\,(1)$ if $+\,(-)$ is taken in (24) and (25).

The eigenvalues $\{\xi(\sigma_1 \dots \sigma_r) : r = 0, \dots, n-1\}$ are obtained from (25) if the initial value $\xi_0 = -3$ is selected (for $r = 0$). The family $\{\eta(\sigma_1 \dots \sigma_r) : r = 0, \dots, n-2\}$ arises from the choice of initial value $\eta_0 = -5$ in (24).

Since each σ_i can take two values, the number of possible eigenvalues in each family, for given r, is 2^r. Therefore, at a level of construction n, the number ν_n of different eigenvalues, including that of the spatially homogeneous state, is

$$\nu_n = \sum_{r=0}^{n-1} 2^r + \sum_{r=0}^{n-2} 2^r + 1 = 3 \times 2^{n-1} - 1. \quad (26)$$

The degeneracy of an eigenvalue $\xi(\sigma_1 \dots \sigma_r)$ at level n is

$$g_n(\xi(\sigma \dots \sigma_r)) = \frac{3^{n-r-1} + 3}{2}, \quad (27)$$

and that of an eigenvalue $\eta(\sigma_1 \dots \sigma_r)$ is

$$g_n(\eta(\sigma_1 \dots \sigma_r)) = \frac{3^{n-r-1} - 1}{2}. \quad (28)$$

Thus, the number of independent eigenmodes is 3^n, as expected:

$$\sum_{r=0}^{n-1} 2^r \left(\frac{3^{n-r-1} + 3}{2}\right) + \sum_{r=0}^{n-2} 2^r \left(\frac{3^{n-r-1} - 1}{2}\right) + 1 = 3^n. \quad (29)$$

The eigenmodes of the coupling matrix reflect the symmetries of the fractal lattice and they are the analogous of the Fourier eigenmodes appearing in regular lattices. The conditions $c_n(\alpha_1 \dots \alpha_r) = 0$ represent different wavelengths on a Sierpinski gasket at a level of construction n.

IV. SCALING PROPERTIES OF THE SPECTRUM

Equations (24) and (25) show that all the eigenvalues $\mu_n(j)$ corresponding to a level of construction n are also eigenvalues at level $n+1$, and that $\mu_n(j) \in [-5, 0]$, $\forall n$. These equations can be seen as a multivalued, one-dimensional map $\mu_{n+1} = y(\mu_n)$, $y : [-5, 0] \to [-5, 0]$, where

$$\mu_{n+1} = y(\mu_n) = \frac{-5 \pm \sqrt{25 + 4\mu_n}}{2}. \quad (30)$$

The inverse mapping

$$\mu_n = z(\mu_{n+1}) = \mu_{n+1}(\mu_{n+1} + 5) \quad (31)$$

has a value $|z(\mu_c)| > 5$ at the critical point μ_c given by $z'(\mu_c) = 0$, therefore almost all points will eventually escape the interval $[-5, 0]$ under iteration of $z(\mu)$. The points that remain in $[-5, 0]$ form a Cantor set, the *repeller* associated with the dynamical system (31). These points coincide exactly with the subset of eigenvalues $\{\eta(\sigma_1 \dots \sigma_r)\}$:

$$z^{(r)}(\mu) = -5 \Rightarrow \mu = \eta(\sigma_1 \dots \sigma_r),$$

$$r = 0, \dots, n-2. \quad (32)$$

The second part of the spectrum of eigenvalues of $\mathbf{M}_n$ is a set of Lebesgue measure zero, given by

$$z^r(\mu) = -3 \Rightarrow \mu = \xi(\sigma_1 \dots \sigma_r), \quad r = 0, \dots, n-1. \quad (33)$$

Figure 2 shows several iterates of the map $z(\mu)$ and the two subsets of eigenvalues of $\mathbf{M}_n$. Figure 3 shows the complete spectrum of eigenvalues of $\mathbf{M}_n$,

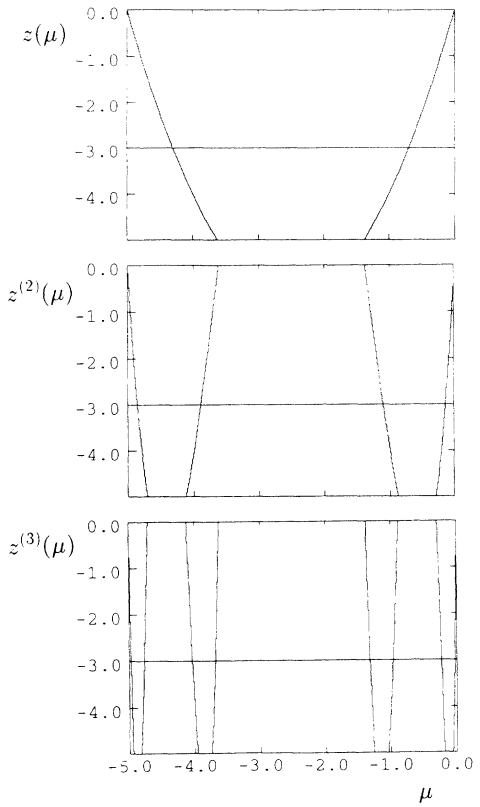

FIG. 2. Iterates of the map $z(\mu) = \mu(\mu + 5)$ on the interval $[-5, 0]$. The eigenvalues $\{\eta_n(\sigma_1 \ldots \sigma_r)\}$ correspond to the intersections of $z^{n+1}(\mu)$ with the μ axis. The eigenvalues $\{\xi_n(\sigma_1 \ldots \sigma_r)\}$ correspond to the intersections with $\mu = -3$.

$$\{\mu_n(j) : j = 1, \ldots, \nu_n\}$$

$$= \{\xi(\sigma_1 \ldots \sigma_r) : r = 0, \ldots, n-1\}$$

$$\bigcup \{\eta(\sigma_1 \ldots \sigma_r) : r = 0, \ldots, n-2\} \bigcup \{0\}, \qquad (34)$$

for $n = 6$, on the μ axis, and the degeneracy of each eigenvalue. Both the distribution of eigenvalues and their degeneracies are nonuniform. The fractal structure is evident in Fig. 3. Another convenient representation of the scaling properties of the spectrum of eigenvalues of the coupling matrix can be achieved by plotting the measure $\sum_j g_n(j)/3^n$ vs $\mu_n(j)$ for large n, as in Fig. 4. The graph so obtained has the characteristics of a *devil's staircase*, a fractal curve that appears in a variety of nonlinear phenomena [10].

Figures 3 and 4 are examples of multifractal measures. A formalism for characterizing the global scaling properties of such objects has been developed [11]. In particular, the part of the complete spectrum of $\mathbf{M}_n$ represented by the subset of eigenvalues $\{\eta(\sigma_1 \ldots \sigma_r) : r = 0, \ldots, n-2\}$ and their degeneracies is a multifractal set, with the repeller associated with (31) as its geometrical support. The number of different elements in this subset is $2^{n-1} - 1$. Let us order them as $\{\eta_n(j'); j' = 1, \ldots, 2^{n-1}\}$, such that $\eta_n(j') < \eta_n(j'')$ if

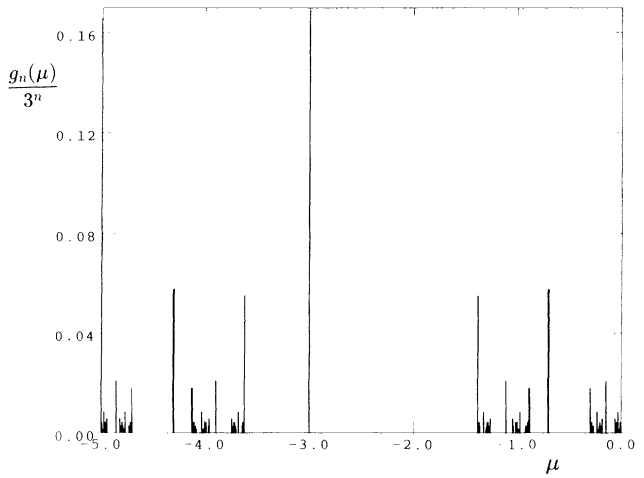

FIG. 3. The spectrum of eigenvalues of $\mathbf{M}_n$, for $n = 6$. The vertical axis shows the degeneracies divided by 3^n.

$j' < j''$, and $\eta_n(1) = 0$ is included. Then the length scales of the repeller at given n are

$$\epsilon_l = |\eta_n(2l-1) - \eta_n(2l)|, \quad l = 1, \ldots, 2^{n-2}. \qquad (35)$$

Each interval ϵ_l contains a number of degenerate eigenvalues

$$g_n(\epsilon_l) = g_n(\eta_n(2l-1)) + g_n(\eta_n(2l)). \qquad (36)$$

The total number of eigenvalues in $\{\eta(\sigma_1, \ldots, \sigma_r) : r = 0, \ldots, n-2\}$ is

$$\sum_{r=1}^{2^{n-2}} 2^r g_n(\eta(\sigma_1 \ldots \sigma_r)) = \frac{1}{2}\left[3^n - 2^{n+1} + 1\right]; \qquad (37)$$

thus the relative probability associated with an interval ϵ_l is

$$p_l = \frac{2g_n(\epsilon_l)}{3^n - 2^{n+1} + 1}. \qquad (38)$$

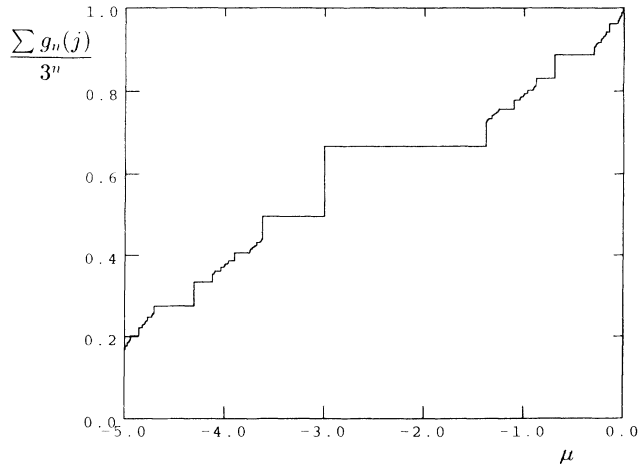

FIG. 4. The measure of the set of eigenvalues of $\mathbf{M}_n$ for $n = 6$.

The multifractal analysis requires the calculation of the partition function [11]

$$\Gamma_n(q,\tau) = \sum_{l=1}^{2^{n-2}} \frac{p_l^q}{\epsilon_l^\tau}, \tag{39}$$

with the condition that $\lim_{n\to\infty}\Gamma_n$ is finite. Equation (39) then determines $\tau(q)$, which can be converted into the $f(\alpha)$ function via a Legendre transform

$$\alpha = \frac{d\tau}{dq}, \quad f = q\alpha - \tau(q). \tag{40}$$

The quantity $f(\alpha)$, called the *spectrum of singularities*, represents the fractal dimension of the subset of the measure for which the probability at length $\epsilon \to 0$ scales as $p(\epsilon) \sim \epsilon^\alpha$.

The spectrum $f(\alpha)$ for the set of eigenvalues $\{\eta(\sigma_1 \ldots \sigma_r) : r = 0, \ldots, n-2\}$ and their degeneracies for large n ($n = 15$) is shown in Fig. 5. The maximum of f corresponds to the fractal dimension of the geometrical support of this set, i.e., to the repeller associated with the map (31). From the calculation, $f_{\max} = 0.551\ldots$. The end points of the $f(\alpha)$ curve $\alpha_{\min}$ and $\alpha_{\max}$ correspond to the scaling exponents of the most concentrated and the most rarified regions of the measure, respectively. In the limit of large n, the length intervals of a repelling set behave as [12]

$$\epsilon_l \sim \left| z^{(n)'}(\eta_n^*(l)) \right|^{-1}, \tag{41}$$

where $\eta_n^*(l)$ are the fixed points of the map $z^{(n)}$ and each interval contains precisely one fixed point. The interval containing the fixed point $\eta_n^* = 0$ has the smallest length, $\epsilon_{\min} \sim 5^{-n}$, and its probability scales as $p_{\min} \sim 3^{-n}$, both for $n \to \infty$. Thus, its corresponding scaling exponent is $\alpha = \ln p_{\min}/\ln \epsilon_{\min} = \ln 3/\ln 5$. The interval containing $\eta_n = -5$ has also length $\epsilon_{\min}$ and the largest probability, which is

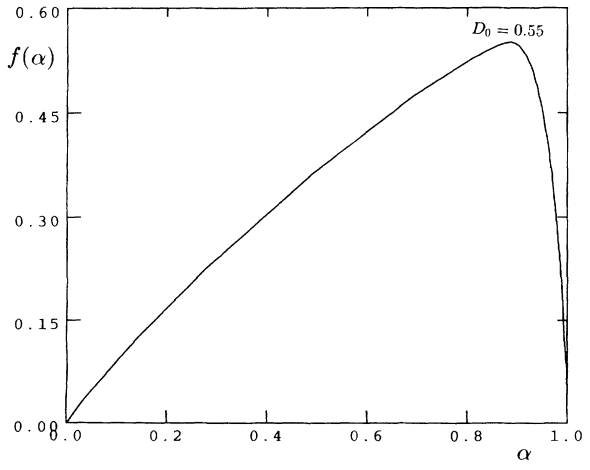

FIG. 5. The spectrum of singularities for the set of eigenvalues of M_n. The maximum of the curve gives the fractal dimension of the repeller associated with the map $z(\mu) = \mu(\mu+5)$.

$$p_{\max} = \frac{3^{n-1}-1}{3^n - 2^{n+1}+1} \longrightarrow \frac{1}{3}, \text{ as } n \to \infty, \tag{42}$$

thus the associated scaling exponent is $\alpha_{\min} = 0$. The maximum value of α is contributed by the largest interval, which is the one containing the fixed point $\eta_n^* = -4$, with length $\epsilon_{\max} \sim 3^{-n}$. Its probability is $p \sim 3^{-n}$, for large n; thus the scaling exponent is $\alpha_{\max} = 1$. These values are verified in Fig. 5.

V. EIGENVALUE MAPS FOR REGULAR LATTICES

The scaling properties of the spectrum of eigenvalues of the matrix expressing diffusion coupling for a fractal lattice differ from those of a regular lattice. The eigenmodes of a regular lattice with periodic boundary conditions are Fourier modes. For a one-dimensional lattice of N elements with periodic boundary conditions and nearest-neighbor coupling, the eigenvalues of the coupling matrix are given by [13]

$$\mu_N(j) = -4\sin^2\left(\frac{\pi j}{N}\right), \quad j = 0, 1, \ldots, N-1. \tag{43}$$

The number of distinct eigenvalues is $N/2$ and each is doubly degenerate. Let $n = 0; 1, 2, \ldots$, be a parameter such that for given n, there are $2^n N$ elements on the lattice. Then if the number of elements is doubled, the following relation can be derived from Eq. (43):

$$\mu_n = \mu_{n+1}(\mu_{n+1} + 4). \tag{44}$$

Equation (44) is a one-dimensional map of the entire interval $[-4, 0]$ onto itself. This corresponds to the condition of fully developed chaos in a quadratic map. The distribution of the iterates is continuous on the interval $[-4, 0]$, and their degeneracy is uniform [7]. Thus, the set of eigenvalues of the coupling matrix does not have a multifractal structure.

For a two-dimensional array of coupled maps with $N_x \times N_y$ elements and periodic boundary conditions in both directions, the eigenvalues of the matrix expressing the diffusive coupling are given by [13]

$$\mu_{N_x,N_y}(k,l) = 2\left[\cos\left(\frac{2\pi k}{N_x}\right) + \cos\left(\frac{2\pi l}{N_y}\right) - 2\right], \tag{45}$$

where $k = 0, 1, \ldots, N_x$; $l = 0, 1, \ldots, N_y$. The number of distinct eigenvalues is $(N_x/2) \times (N_y/2)$, and their degeneracy for given k and l is 4. Define

$$\theta_{N_y}(l) = \cos\left(\frac{2\pi l}{N_y}\right) - 2, \tag{46}$$

and let $n = 0, 1, \ldots$ be a parameter such that for given n, there are $2^n N_x \times 2^n N_y$ coupled elements on the array. Then, Eq. (45) can be written as a two-dimensional map:

$$\begin{aligned} \mu_n &= \mu_{n+1}(\mu_{n+1} - 4\theta_n) + 2(\theta_n + 1)(2\theta_n - 1), \\ \theta_n &= 2\theta_{n+1}(\theta_{n+1} + 4) + 5. \end{aligned} \tag{47}$$

The equation for θ_n maps the interval $[-3, -1]$ onto itself.

For $\theta_n \in [-3,-1]$, the equation for μ_n maps the interval $[a,b]$ onto itself, where $a = 2\theta_n - 2, b = 2\theta_n + 2$, and $|b-a| = 4$. Therefore the distribution of iterates on the interval $[a,b]$ is continuous. Since the degeneracies of the eigenvalues are constant, the distribution of degeneracies is uniform, and the set of eigenvalues of the coupling matrix does not have a multifractal structure.

VI. STABILITY AND BIFURCATION OF SYNCHRONIZED STATES

The synchronized, period-doubling attractors of CML's possess a scaling structure [13,14] which is a generalization of that of Feigenbaum [15] for single maps. Below we utilize the results of previous sections to derive this structure for CMFL's of maps with quadratic extrema.

Like coupled maps on regular lattices with diffusion coupling, the system described by Eqs. (2a) or (2b) has the characteristic feature that the coupling term vanishes for the spatially synchronized states. These states are relevant since one is often interested in the mechanism by which a uniform system breaks its symmetry to form a spatial pattern as a bifurcation parameter is varied. We consider Eq. (2a) for backward diffusion coupling. The analysis of the bifurcation structure can be carried out by the following transformation of coordinates. Let $\mathbf{U}_n$ be the orthogonal matrix that diagonalizes $\mathbf{M}_n$. The jth column of $\mathbf{U}_n$ consists of the components of the eigenvector $\mathbf{u}_n(j)$: $U_n(i,j) = [\mathbf{u}_n(j)](i)$. Introduce the change of coordinates $\boldsymbol{\phi}_n = \mathbf{U}_n^{-1}\mathbf{x}_n$, $\mathbf{x}_n = \mathbf{U}_n\boldsymbol{\phi}_n$; that is,

$$\phi_n(i;t) = \sum_j U_n(j,i)x_n(j;t),$$
$$x_n(i;t) = \sum_j U_n(i,j)\phi_n(j;t), \tag{48}$$

and define

$$\hat{f}(\phi_n(i;t)) = \sum_j U_n(j,i) f\left(\sum_j U_n(i,j)\phi_n(j;t)\right). \tag{49}$$

In the $\{\phi_n(i)\}$ coordinates, Eq. (2a) becomes

$$\phi_n(i;t+1) = \hat{f}(\phi_n(i;t);\lambda) + \gamma\mu_n(i)\phi_n(i;t). \tag{50}$$

The spatially synchronized, period-N states $x_n(i) = \overline{x}_k$ $(k = 1,\ldots,N)$, $\forall i$ are given by the solutions of

$$f^{(N)}(\overline{x}_k,\lambda) = \overline{x}_k, \tag{51}$$

and their stability can be examined in terms of the $\{\phi_n(i)\}$ coordinates [13]. The linear stability analysis of the periodic, synchronized states leads to

$$S_n^{(N)}(j) = \prod_{k=1}^{N}[f'(\overline{x}_k,\lambda) + \gamma\mu_n(j)] = \pm 1. \tag{52}$$

Equations (52) yield boundary curves in the $\lambda\gamma$ plane which determine the stability regions of the period N, synchronized states.

The boundary curves depend on the coupling only through the product $\gamma\mu_n(j)$. Thus, for a particular f, the generic curves $S_n^{(N)} = +1$ and $S_n^{(N)} = -1$ may be obtained by plotting λ vs $\gamma\mu$. At a level of construction n there are ν_n different values of $\mu_n(j)$ to consider. Thus for a particular f, each generic boundary curve is split into ν_n curves in the $\lambda\gamma$ plane, which may be obtained from the original by changing $\mu_n(j)$.

The splitting of the boundary curves according to the level of construction has important consequences for the stability regions of the synchronized states on a fractal lattice. As an example, consider $f(x) = \lambda x(1-x)$ (logistic map). Then the bifurcation condition, Eq.(52), for the period-$(N = 2^m)$ synchronized state becomes

$$S_n^{(m)}(\mu(j)) = \prod_{k=1}^{2^m}[\lambda(1-2\overline{x}_k) + \gamma\mu_n(j)] = \pm 1. \tag{53}$$

Figure 6 shows the boundary curves $S_3^{(1)} = \pm 1$ in the $\lambda\gamma$ plane (for the period-2 synchronized state), which are given by

$$-\lambda^2 + 2\lambda + 4 + \gamma\mu_3(j)[\gamma\mu_3(j) - 2] = \pm 1,$$
$$\nu_3 = 11; \qquad j = 1,2,\ldots,11. \tag{54}$$

The upper curves $S_3^{(1)}(\mu(j)) = -1$ have minima $\lambda_{\min} = 1+\sqrt{5}$ at values $\gamma_3(j)_{\min} = 1/\mu_3(j)$. Around those minima, these boundary curves are approximated by parabolas

$$\lambda \approx \lambda_{\min} + \frac{1}{2\sqrt{5}}[\gamma\mu_n(j) - 1]^2. \tag{55}$$

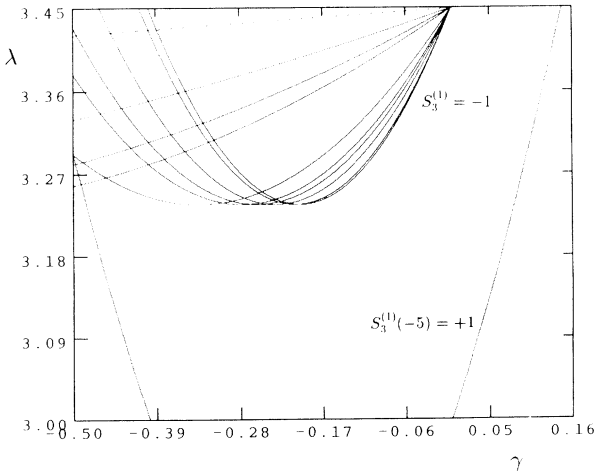

FIG. 6. The boundary curves $S_3^{(1)} = \pm 1$ for the period-2 synchronized states of a Sierpinski gasket at level $n = 3$. The interior region defined by these curves is where stable, synchronized, period-2 orbits exist in the $\lambda\gamma$ plane.

Equation (55) is valid for any period 2^m, with $\lambda_{\min}$ depending on m. Figure 7 is a magnification of Fig. 6 around the minima of the curves $S_3^{(1)}(\mu(j))$. The fractal structure of the eigenvalues $\mu_n(j)$ is reflected in the distribution of the minima $\gamma_n(j)$ and in the presence of nonuniform gaps (niches) in the boundary curves at any level n. This feature allows for regions of stability for the synchronized states that are not present in regular lattices, where the distribution of eigenvalues of the coupling matrix is uniform.

Although the distribution of eigenvalues $\mu_n(j)$ differs for fractal and regular lattices, the form of Eq. (53) is the same. Consequently, the scaling structure for the period 2^n, synchronized states is similar in both cases. Figure 6 shows the stability regions of the period-2 synchronized state in the $\lambda\gamma$ plane. The corresponding regions for synchronized period-2^n states can be obtained by scaling λ by δ^{-n} and γ by α^{-n}, where $\delta = 4.669\ldots$ and $\alpha = -2.5029\ldots$ are Feigenbaum's scaling parameters [13]. Thus the image of Fig. 6 is reduced and reflected about $\gamma = 0$ for the higher periods. The same is true for regular lattices; it is the shape of the scaled regions that changes for fractal lattices.

The eigenvectors $\{\mathbf{u}_n(i)\}$ constitute a complete basis (normal modes) and the state $\mathbf{x}_n(t)$ of the system can be represented as a linear combination of these vectors. Thus

$$\mathbf{x}_n(t) = \sum_{j=1}^{\nu_n} \sum_{k=1}^{g_n(j)} a_j^{(k)}(t)\mathbf{u}_n^{(k)}(j). \tag{56}$$

The evolution of $\mathbf{x}_n(t)$ then reflects the stabilities of the normal modes. Figure 7 shows how the synchronized state may become unstable through crossing of the boundary curves for the $\mathbf{u}_n^{(k)}(j)$ modes; the first boundary crossed determines the character of the instability. In regular Euclidean lattices, the minima $\gamma_{\min}$ of the

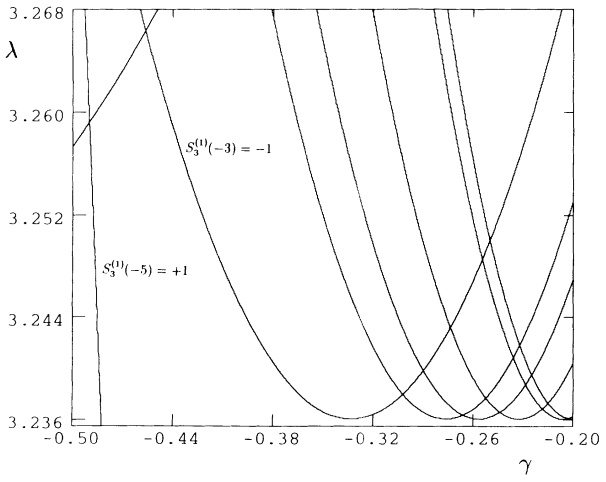

FIG. 7. A magnification of Fig. 6 showing the gaps in the stability boundary of the period-2, synchronized states. The fractal structure of the eigenvalues of $\mathbf{M}_n$ allows regions of stability that are not present in regular lattices.

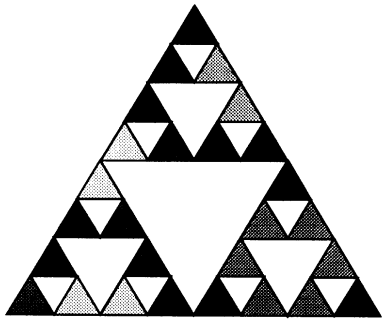

FIG. 8. Inhomogeneous state at parameter values $\lambda = 3.245, \gamma = -0.4$. This state is a linear combination of the six eigenmodes corresponding to the eigenvalue $\mu = -3$, at a level $n = 3$.

$S_n^{(m)} = -1$ curves will cover the whole of the interval $[-\infty, -0.25]$ on the γ axis (one-dimensional lattice) or the interval $[-\infty, -0.125]$ (two-dimensional lattice), for $n \to \infty$, for any period 2^m. Therefore, by crossing along either interval, the synchronized state will bifurcate into a superposition of many unstable modes, producing in general a complex spatiotemporal pattern. Because of the niches in the stability boundaries at any level n, it is possible for the coupled-map system on a fractal lattice to evolve from a spatially homogeneous state into a state with a spatial pattern determined by a pure (degenerate) mode. To see this, consider an initial condition consisting of a small perturbation of the homogeneous, period-2 state at parameter values just beyond the boundary $S_3^{(1)}(-3) = -1$, where this initial state is unstable. The final state is pictured in Fig. 8. It corresponds to a linear combination of the $g_3(-3) = 6$ eigenmodes $\mathbf{u}_3^{(k)}(j)$, $k = 1, \ldots, 6$, for $\mu(j) = -3$. All other modes are unstable in this region of parameter space. For any level of construction n, and any period 2^m, the curve $S_n^{(m)}(-3) = -1$ separates a niche of the synchronized state from the stable region for the $\mathbf{u}_n^{(k)}(j)$ modes corresponding to $\mu(j) = -3$. Thus, a transition between these two spatial patterns can always be observed in the appropriate regions of the $\lambda\gamma$ plane.

VII. DISCUSSION

The inhomogeneous structure of the Sierpinski gasket on which the coupled-map system is defined gives rise to a number of features which affect the bifurcations of this dynamical system. The scaling structure of the synchronized, period-doubled states is similar for both regular and fractal lattices but the nature of the bifurcation boundaries is different. For the fractal lattice, the boundary curves are determined by the spectrum of eigenvalues of the diffusion coupling matrix, which is a multifractal. The nonuniform distribution of eigenvalues leads to niches in the boundary curves that are not present for coupled maps on regular lattices, where the eigenvalue distribution is continuous. The fractal normal modes determine the inhomogeneous spatial structures in the

vicinity of these boundary curves, and states with relatively simple inhomogeneous character can be found in bifurcations of the synchronized states within the niches.

A number of generalizations and extensions of this work are possible. We have examined only the simplest spatiotemporal states on a fractal lattice. The extensions of phenomena like intermittency and other forms of spatiotemporal chaos to the fractal domain can be investigated. Also, problems related to competition between stable states and domain evolution in discrete dynamical systems involve new features when compared with the corresponding processes on regular lattices. Some aspects of domain formation and growth on the Sierpinski gasket are similar to those for the segregation of species observed in random-walk models of bimolecular reactions on fractals [6] and have their origin in the poor diffusion mixing on the fractal lattice.

The study of coupled maps on fractal lattices should allow one to gain insight into a previously unexplored range of spatiotemporal phenomena and provide a basis for the construction of simulation algorithms for the dynamics of these systems.

ACKNOWLEDGMENTS

This work was supported in part by a grant from the Natural Sciences and Engineering Research Council of Canada.

[1] For reviews, see J. P. Crutchfield and K. Kaneko, in *Directions in Chaos I*, edited by Hao Bai-Lin (World Scientific, Singapore, 1987); K. Kaneko, *Physica D* **34**, 1 (1989); K. Kaneko, in *Formation, Dynamics and Statics of Patterns*, edited by K. Kawasaki (World Scientific, Singapore, 1989); R. Kapral, *J. Math. Chem.* **6**, 113 (1991); R. Kapral, in *Self-Organization, Emerging Properties and Learning*, edited by A. Babloyantz (Plenum, New York, 1991), p. 31.

[2] Some examples of this type of application can be found in R. Kapral , in *Theory and Applications of Coupled-Maps Lattices*, edited by K. Kaneko (Manchester University Press, Manchester, 1992); T. Bohr, A. W. Pedersen, M. H. Jensen, and D. Rand, in *New Trends in Nonlinear Dynamics and Pattern Forming Processes*, edited by P. Coullet and P. Heurre (Plenum, New York, 1989); D. Barkley, M. Kness, and L. Tuckerman, Phys. Rev. A **42**, 2489 (1990); D. Barkley, Physica D **49**, 61 (1991); R. Elder, T. M. Rogers, and R. C. Desai, Phys. Rev. B **38**,4725 (1988); Y. Oono and S. Puri, Phys. Rev. Lett. **58**, 836 (1987).

[3] B. B. Mandelbrot, *The Fractal Geometry of Nature* (Freeman, New York, 1982).

[4] Y. Gefen, B. B. Mandelbrot, and A. Aharony, Phys. Rev. Lett. **45**, 855 (1980).

[5] R. Rammal and G. Toulouse, J. Phys. (Paris) Lett. **44**, L13 (1983).

[6] R. Kopelman, Science **241**, 1620 (1988); G. Zumofen, J. Klafter, and A. Blumen, Phys. Rev. A **43**, 7068 (1991); B. J. West, R. Kopelman, and K. Lindenberg, J. Stat. Phys. **54**, 1429 (1989); and for additional applications, *The Fractal Approach to Heterogeneous Chemistry*, edited by D. Avnir (Wiley, New York, 1989).

[7] R. Rammal, J. Phys. (Paris) **45**, 191 (1984).

[8] The three-vertex cells are the only boundary cells in the Sierpinski gasket so specific boundary conditions need not be introduced.

[9] S. Alexander and R. Orbach, J. Phys. (Paris) Lett. **43**, 625 (1982).

[10] P. Bak, Phys. Today **39**, 38 (1986).

[11] T. C. Halsey, M. H. Jensen, L. P. Kadanoff, I. Procaccia, and B. I. Shraiman, Phys. Rev. A **33**, 1141 (1986).

[12] T. Bohr and D. Rand, Physica D **25**, 387 (1987).

[13] I. Waller and R. Kapral, Phys. Rev. A **30**, 2047 (1984); R. Kapral, *ibid.* **31**, 3868 (1985).

[14] S. P. Kuznetsov and A. S. Pikovsky, Physica D **19**, 384 (1986).

[15] M. J. Feigenbaum, J. Stat. Phys. **19**, 25 (1978); **21**, 669 (1979).

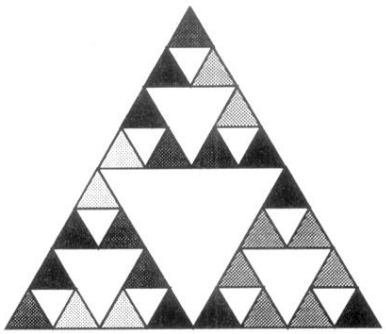

FIG. 8. Inhomogeneous state at parameter values $\lambda = 3.245, \gamma = -0.4$. This state is a linear combination of the six eigenmodes corresponding to the eigenvalue $\mu = -3$, at a level $n = 3$.